14. Uluslararası Makina Tasarım ve İmalat Kongresi
29 Temmuz – 02 Eylül 2010, Güzelyurt, KKTC

PROCESS SIMULATION FOR 5-AXIS MACHINING USING GENERALIZED MILLING TOOL GEOMETRIES

Ömer M. ÖZKIRIMLI, *ozkirimli@sabanciuniv.edu,* Sabancı University, Manufacturing Research Laboratory, 34956, İstanbul

Erhan BUDAK, *ebudak@sabanciuniv.edu,* Sabancı University, Manufacturing Research Laboratory, 34956, İstanbul

ABSTRACT

Multi-axis machining (especially 5-axis machining) is widely used in precision machining for automotive, aerospace and die-mold manufacturing. The goal in precision machining is to increase production while meeting high part quality needs which can be achieved through decision of appropriate process parameters considering machine tool constraints (such as power and torque), chatter-free operations and part quality. In order to predict and decide on optimal process parameters, simulation models are used. In the literature, individual tool geometries for multi-axis machining are examined in detailed with different modeling approaches to simulate cutting forces. In this study, a general numerical model for 5-axis machining is proposed covering all possible tool geometries. Tool envelope is extracted from CAD data, and helical flutes points are represented in cylindrical coordinates. Equal parallel slicing method is utilized to find cutter engagement boundaries (CEB) determining cutting region of the tool surface. for each axial level in the tool axis direction. For each level uncut chip thickness value is found and total forces are calculated by summing force values for each point along the cutting flutes. For arbitrary cases forces are simulated and obtained results are experimentally verified.

Keywords: Multi-axis machining, APT tools, Process simulation, Tool engagement

1. INTRODUCTION

Milling is widely used in manufacturing operations. Milling tools may have different geometries chosen for area of application. Precision manufacturing requires adjusting process parameters appropriately to eliminate failures and scraping parts. Poor choices may

result in stall of the machine tools, excessive part and tool deflection or tool breakages due to high cutting forces. In prediction of optimal cutting parameters process models and simulations can be employed. Mechanics of milling have been extensively analyzed in the past. Researchers first investigated the geometry of milling tools and milling mechanics [Martelotti, 1941; Koenigsberger and Sabberwal, 1961]. Kline et al. constructed a mechanistic model based on chip load, cutting geometry and presented average forces in terms of feed rate and cutting parameters [1982]. Altintas and Spence [1991] investigated end milling process and presented a semi-analytical algorithm to be integrated in CAD systems. Both mechanics and dynamics of milling process were studied by Altintas and Lee [1996]. Altintas and Engin [2001] presented a process model for general cutter geometries. Upon this research Gradisek et. al. [2004] presented a method to identify force coefficients for a general end mill where it is possible to obtain a closed form analytical formulation for average cutting forces. Finally, Altintas and Merdol [2008] extended previously proposed methods and obtained an analytical force expression for general cutting tools in for 2.5D milling operations.

The research on multi-axis milling has been relatively limited. Process models were first developed for sculptured surface machining with ball-end tools for 3-axis machining [Lazoğlu and Lyang, 2000]. For multi-axis machining, the most crucial part is to construct a reliable cutter-workpiece engagement model for which several approaches have been introduced. Digitization of the in cut workpiece yields accurate results, however suffers from computational load and memory usage. Digitization algorithms include widely used Z-mapping [Kim, 2000; Maeng, 2003] where workpiece in cut is modeled using surface normal vector with associated cut heights, whereas in octree method [Kim and Ko, 2006] workpiece is meshed, and the intersecting meshes are divided into sub meshes for accuracy. On the other hand, more accurate results are obtained using analytical approaches [Ozturk and Budak, 2007] where a robust model is formed, but only several arbitrary processes with ball end mills can be analyzed. Process models for taper ball end mills which are extensively used in aerospace industry for airfoil machining were constructed with a semi-analytical method involving parallel slicing of the workpiece [Ferry and Altintas, 2008]. Today, a complete process model for multi-axis machining where different tool types can be investigated for intricate tool geometries is missing.

In this paper, a numerical process model is proposed for general tool geometries covering a very wide range of practical tools used in industry. The new model introduce a simple methodology to identify cutter-workpiece engagement region by identifying the peripheral cutter points lying in the process boundary defined by the process parameters in workpiece coordinates. The process boundary is identified employing Boolean operations to find the

union of three separate boundary conditions which are axial, radial and chip normal direction boundaries. Finally, the engagement boundary is represented on the tool surface find cutting segments to be evaluated. Forces are then calculated using linear mechanistic model with respect to chip load and differential cutting edge segment lengths. The proposed model is compared with experimental data.

2. Geometry of a general milling cutter

Various types of helical milling cutters are used in machining operations chosen according to the area of application and geometry of the surface to be machined. For example, ball end mills are used in die finishing, taper ball end mills are used in flank milling of compressor blade surfaces and bull nose mills are used for sculptured surface milling. In order to evaluate cutting forces, cutting edge geometry must be known. Tool envelope of general milling cutters can be identified using APT representation consisting of seven geometric parameters which are $D, R, R_r, R_z, \alpha, \beta, H$ as shown Fig. 1. A general end mill can be divided into three main segments which are the tip part shown by line [OM] with inclination angle α, the torus part shown by arc [MN] with center point *C* and radius R and the taper part shown by line [NS] with taper angle β. According to assigned tool parameters some of these segments may vanish. Engin and Altintas [1996] investigated general milling tool geometries and proposed a complete model to analytically present tool envelope and helical flutes in tool coordinate system.

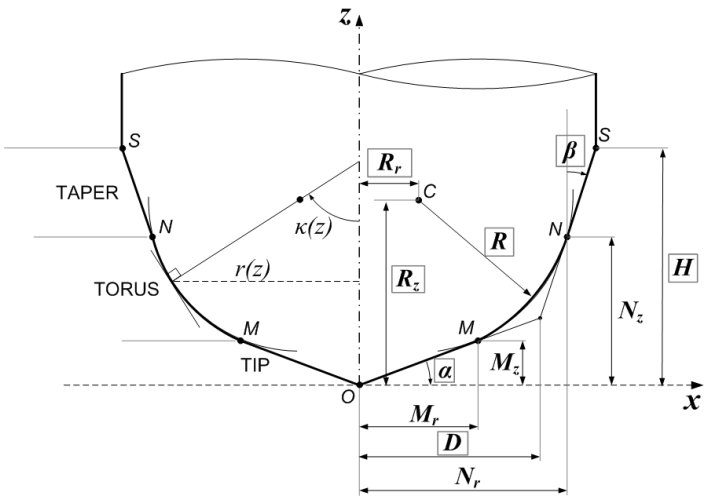

Fig. 1. Geometry of general milling cutters with APT parameters

In this study, the tool envelope is constructed in CAD environment and converted to 2D IGES data from which required tool parameters are extracted. Initial Graphics Exchange

Specification (IGES) is an ASCII based data format where construction elements of a solid or drawing is presented separately regarding the type [National Bureau of Standarts, 1980]. A typical IGES file representing the cutter boundaries contains line and arc arrays defining each segment of the tool envelope as shown in Fig. 2.

```
110,0.,0.,0.,3.,0.528980942,0.;                                    3P
100,0.,2.479055467,3.483404201,3.,0.528980942,5.433478726,         5P
2.962459668;                                                       5P
110,5.433478726,2.962459668,0.,7.556021868,15.,0.;                 7P
```

Fig. 2. IGES file portion showing general tool segment definitions

Each array starts with the type definition of the corresponding segment being arc or line, and following numbers designates the start, end and arc center points in the tool coordinate system. These boundary points provide the information about the position of the envelope transition point and arc center points (*O,N,M,S* and *C*) shown in Fig. 1.

Mechanistic approach of cutting process requires the local cutting edge geometry and the chip load to determine forces acting on cutting points along the flutes. A point P on a helical cutting flute is defined in cylindrical coordinates by characterizing radial distance $r(z)$, the axial immersion angle $\kappa(z)$ being the angle between the tool axis and the normal vector of the cutting edge and the radial lag angle $\psi(z)$ being the difference of the radial immersion angle with respect to the start point of the cutter due to the helical cutting flutes (**Fig. 3**). For each segment of the cutter envelope at each elevation level z radial distance and immersion angle are defined as follows;

$$\left.\begin{aligned} r(z) &= \frac{z - M_z}{\tan\alpha} \\ \kappa(z) &= \alpha \end{aligned}\right\} \quad \text{for TIP part (OM)}$$

$$\left.\begin{aligned} r(z) &= \sqrt{R^2 - (R_z - z)^2} + R_r \\ \kappa(z) &= \sin^{-1}\left(\frac{r(z) - R_r}{R}\right) \end{aligned}\right\} \quad \text{for TORUS part (MN)} \qquad (1)$$

$$\left.\begin{aligned} r(z) &= N_r + (z - N_z)\tan\beta \\ \kappa(z) &= \frac{\pi}{2} - \beta \end{aligned}\right\} \quad \text{for TAPER part (NS)}$$

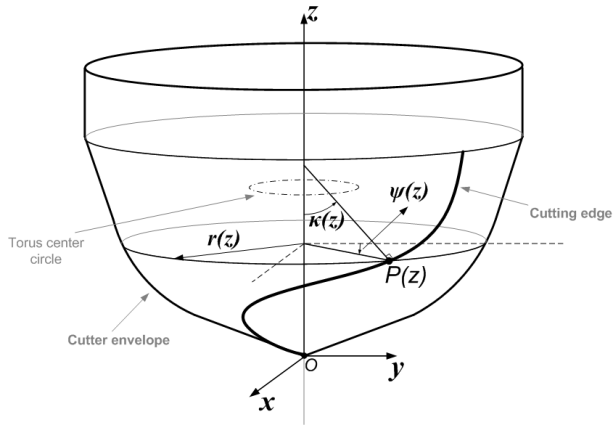

Fig. 3. 3D representation of the general milling cutter

Due to helical cutting flutes, cutting points at different elevations are shifted rotationally along the periphery of the cutter body with respect to each other. This rotational shift at elevation z is defined as the lag angle, $\psi(z)$. The lag angle varies from segment to segment due to the change in the geometry of the profile. The lag angle at the tip conical part, designated by line [OM], for a given helix angle i_0 is defined as follows;

$$\psi(z) = \psi_{TIP}(z) = \frac{\ln(z\cot\alpha)\tan i_0}{\cos\alpha} \tag{2}$$

For the torus section, the lag angle deviation (3) and the lag angle for a point at the torus segment are defined in (3) and (4) as follows:

$$\psi_{TORUS}(z) = \frac{(R+z-R_z)\tan i_0}{R} \tag{3}$$

$$\psi(z) = \psi_{TORUS}(z) - \psi_{TORUS}(M_z) + \psi_{TIP}(M_z) \tag{4}$$

In the taper segment, tools may have constant helix similar to the lower segment or constant lead resulting in variable helix angle. For the constant helix case, the lag angle definition is as follows:

$$\psi_{TAPER_{helix}}(z) = \frac{\ln(N_r - (N_z - z)\tan\beta)\tan i_0}{\sin\beta} \tag{5}$$

$$\psi(z) = \psi_{TAPER-helix}(z) - \psi_{TAPER-helix}(N_z) + \psi_{TORUS}(N_z) \tag{6}$$

Variable helix angle, i_s, due to constant lead defined by pitch length, p_l, can be calculated as follows:

$$i_s = \tan^{-1}\left(\frac{2\pi N_r}{p_l \cos\beta}\right) \tag{7}$$

Accordingly, the lag angle of a point in the taper zone with constant lead is defined as;

$$\psi(z) = \underbrace{\frac{(z - N_z)\tan i_s}{N_r}}_{\psi_{TAPER-lead}(z)} + \psi_{TORUS}(N_z) \tag{8}$$

In Fig. 4 some sample tool envelopes extracted from IGES data and constructed in 3D with helical flutes are demonstrated.

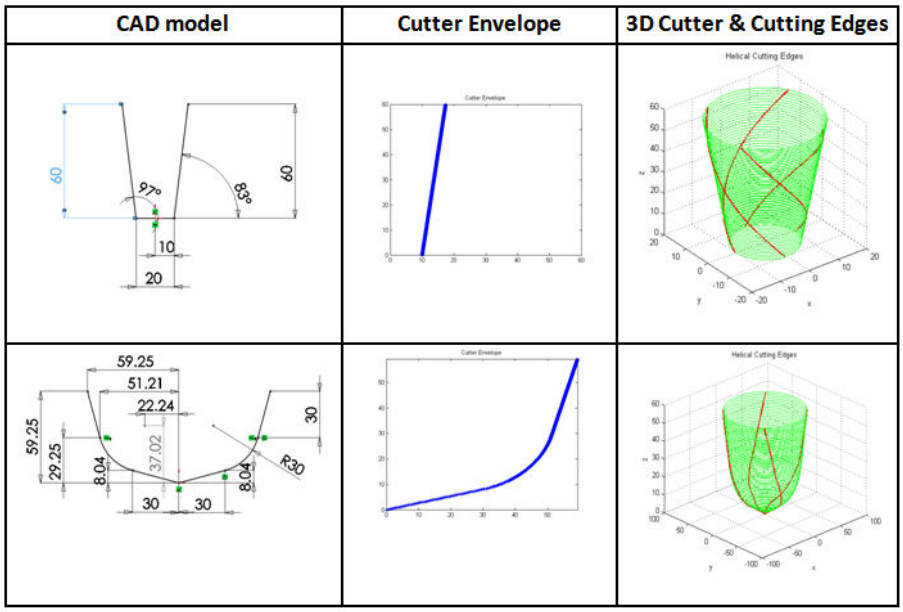

Fig. 4. Example cutter representations with helical flutes

3. Process Model

In cutting operations, the forces acting on the tool are calculated using a process model based on the chip load and engagement boundaries of the tool. In the below schematic, the process tree is shown. The procedure involves first to identify the cutting edge geometries in cylindrical coordinates from the given tool parameters and to calculate engagement zones at each cross-section along tool axis from process parameters, i.e. the tool rotation angles, depth of cuts and feed direction, in order to calculate the flute segments in cut. Finally, differential cutting forces acting on the cutting edge point are calculated employing linear mechanistic model requiring the cutting force coefficients, the chip load and the length of the cutting edge.

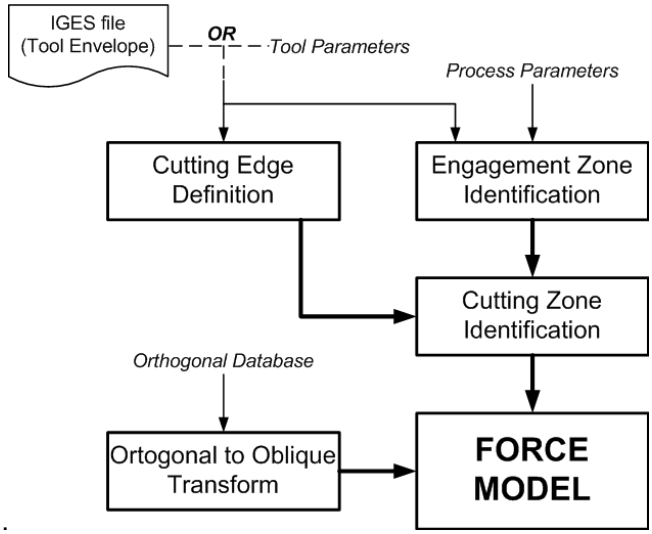

Fig. 5. Process model schematic

Tool orientation and position in 5-axis milling

In multi-axis machining, the tool axis and the machine table normal are not parallel to each in the presence of rotation angles. Workpiece surface coordinates along tool path direction are considered as the process coordinates which is designated by FCN where F defines the feed direction along the tool path, C is the cross-feed direction and N is the surface normal direction. Tool rotation angles are defined with respect to the rotations around these coordinates. Lead angle is defined as the rotation about cross-feed direction C whereas tilt angle is the rotation about the feed direction as shown in Fig. 6. T_{FCN} defines the Euler transformation for lead and tilt rotations represented as l and t:

$$T_{FCN} = \begin{bmatrix} 1 & 0 & 0 \\ 0 & \cos t & -\sin t \\ 0 & \sin t & \cos t \end{bmatrix} \begin{bmatrix} \cos l & 0 & \sin l \\ 0 & 1 & 0 \\ -\sin l & 0 & \cos l \end{bmatrix} \tag{9}$$

Moreover, cutter tip point, *CL* defining the cutter location must be translated due to cutter rotations in order to position the tool tangent to the machined surface. FN plane in process coordinates is considered as the surface to be machined, and FCN coordinate is fixed at the cutter contact location, *CC,* which is the lowermost point of the cutter envelope on FN plane. CL point location in FCN coordinates (Fig. 7) can be expressed as the sum of the vectors $\mathbf{t}_1$, $\mathbf{t}_2$ and $\mathbf{t}_3$ as follows [Choi and Jerard, 1998] :

$$CL_{FCN} = \mathbf{t}_1 + \mathbf{t}_2 + \mathbf{t}_3 \tag{10}$$

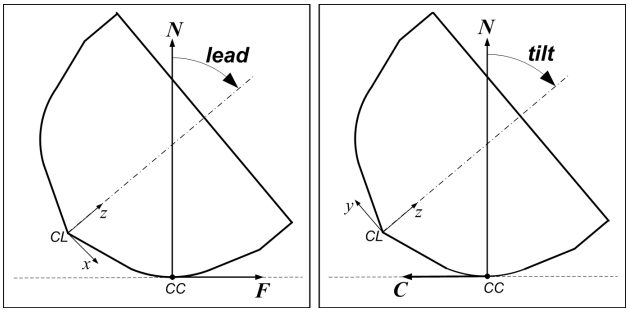

(a) (b)

Fig. 6 (a) Lead and (b) tilt angle representations

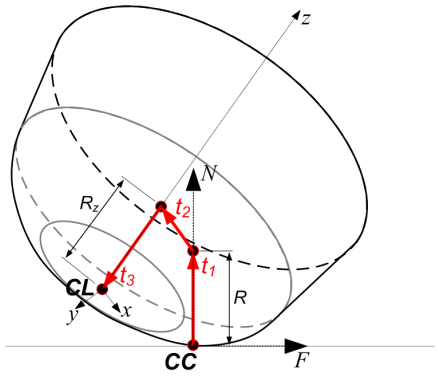

Fig. 7. CL point representation in process coordinates.

The translation vectors are defined as follows:

$$\left.\begin{aligned} \mathbf{t_1} &= R \cdot \hat{\mathbf{N}} \\ \mathbf{t_2} &= R_r \cdot \frac{\left(\hat{\mathbf{N}} \times \hat{\mathbf{z}}\right) \times \hat{\mathbf{z}}}{\left\| \left(\hat{\mathbf{N}} \times \hat{\mathbf{z}}\right) \times \hat{\mathbf{z}} \right\|} \\ \mathbf{t_3} &= -R_z \cdot \hat{\mathbf{z}} \end{aligned}\right\} \tag{11}$$

A point in the tool axis, xyz can be represented in the process coordinates FCN as follows:

$$\begin{bmatrix} F \\ C \\ N \end{bmatrix} = T_{FCN} \cdot \begin{bmatrix} x \\ y \\ z \end{bmatrix} + \begin{bmatrix} CL_F \\ CL_C \\ CL_N \end{bmatrix} \tag{12}$$

A point on the cutter body defined in cylindrical coordinates with respect to tool axis can be represented in process coordinates as follows:

$$\begin{bmatrix} P_F \\ P_C \\ P_N \end{bmatrix} = T_{FCN} \cdot \begin{bmatrix} r(z)\cos\left(\pi - \phi_j(z)\right) \\ r(z)\sin\left(\pi - \phi_j(z)\right) \\ z \end{bmatrix} + \begin{bmatrix} CL_F \\ CL_C \\ CL_N \end{bmatrix} \tag{13}$$

Mechanistic force model

In order to calculate the cutting forces acting on the flutes, differential cutting elements are analyzed using oblique cutting mechanics. In Fig. 8, the cutting forces acting on a point on the j[th] cutting edge are shown. A point on a cutting flute, *P,* is designated in cylindrical coordinates by its elevation from the tool tip along tool axis, z, and the radial immersion $\phi_j(z,\phi)$. Axial immersion angle is defined as follows:

$$\phi_j(z) = \phi + \phi_{p_j} - \psi(z) \tag{14}$$

where ϕ is the rotation angle of the tool around the tool axis, $\psi(z)$ is the lag angle at point *P,* and ϕ_{p_j} is the pitch angle. Differential cutting forces in the radial, axial and tangential directions on a cutting edge point of the j[th] tooth at elevation z and radial rotation ϕ_j are calculated according to the model proposed by Lee and Altintas [1996] (Fig. 8) as follows:

$$\begin{bmatrix} dF_{r_j}(z) \\ dF_{t_j}(z) \\ dF_{a_j}(z) \end{bmatrix} = \begin{bmatrix} K_{rc}h(\phi_j,z)db + K_{re}dS \\ K_{tc}h(\phi_j,z)db + K_{te}dS \\ K_{ac}h(\phi_j,z)db + K_{ae}dS \end{bmatrix} \cdot \delta(z) \quad \text{where } j = 1,\ldots,N_f \tag{15}$$

where K_{rc}, K_{tc}, K_{tc} and K_{re}, K_{te}, K_{te} are the cutting force are the edge force coefficients determined from orthogonal cutting database using the oblique transformation (Budak et al. [1996]). Chip thickness $h(\phi,z)$ and chip width db define the chip area in contact with the cutting flute whereas differential cutting edge length dS is required for edge forces. . Finally, $\delta(z)$ is the Boolean function designating whether the point of interest is in cut or not:

$$\delta(z) = \begin{cases} 1 & \text{if } P(z,\phi_j) \in CEB(z) \\ 0 & \text{if } P(z,\phi_j) \notin CEB(z) \end{cases} \tag{16}$$

If the point is in cut it must be within the cutter engagement boundary (CEB). Chip thickness is the thickness of the material removed in the normal direction of the cutting flute:

$$h(\phi,z) = \mathbf{n} \bullet \mathbf{f} \tag{17}$$

where $\mathbf{f}$ vector is the feed direction vector in tool coordinates and $\mathbf{n}$ is the unit outward surface normal vector at point *P*. Unit outward vector is defined in terms of axial immersion and radial immersion angles as follows:

$$\mathbf{n} = \begin{bmatrix} \sin\kappa \sin\phi_j \\ \sin\kappa \cos\phi_j \\ -\cos\kappa \end{bmatrix} \tag{18}$$

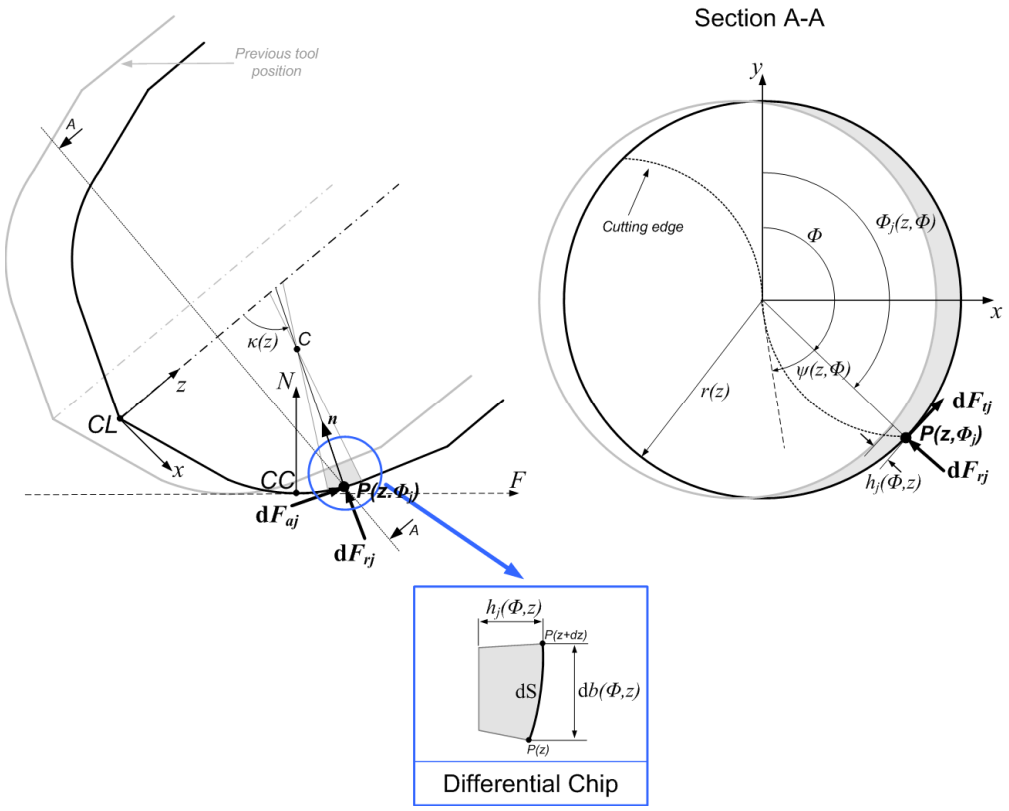

Fig. 8. Mechanics of multi-axis machining

Chip width is defined as the length of the tangent line of the cutting envelope for a differential axial length:

$$\mathrm{d}b = \frac{\mathrm{d}z}{\sin\kappa(z)} \tag{19}$$

Edge forces are originated from the plowing mechanism during machining. Cutting edge length at elevation z with differential axial element length dz is expressed as follows:

$$\mathrm{d}S = \begin{Vmatrix} P_x(z) - P_x(z-\mathrm{d}z) \\ P_y(z) - P_y(z-\mathrm{d}z) \\ P_z(z) - P_z(z-\mathrm{d}z) \end{Vmatrix} \tag{20}$$

The tangential, radial and axial forces are resolved in tool coordinates considering a transformation in terms of axial and radial immersion angles, κ and ϕ:

$$\begin{bmatrix} F_x \\ F_y \\ F_z \end{bmatrix} = T \cdot \begin{bmatrix} F_r \\ F_t \\ F_a \end{bmatrix} \quad \text{where} \quad T = \begin{bmatrix} -\sin\phi_j \sin\kappa & -\cos\kappa & -\sin\phi_j \cos\kappa \\ -\cos\phi_j \sin\kappa & \sin\kappa & -\cos\phi_j \cos\kappa \\ -\cos\kappa & 0 & -\sin\kappa \end{bmatrix} \tag{21}$$

The total milling forces in tool coordinates at a radial immersion ϕ is the summation of the contributions from all teeth in cut:

$$F_k(\phi) = \sum_{j=1}^{N_f} \sum_{i=0}^{L/dz} \left(dF_{kj}\left(\phi(i \cdot dz)\right)\right) \qquad k = x, y, z \tag{22}$$

Finally, total forces are expressed in process coordinates as follows:

$$\begin{bmatrix} F_F \\ F_C \\ F_N \end{bmatrix} = T_{FCN} \cdot \begin{bmatrix} F_x \\ F_y \\ F_z \end{bmatrix} \tag{23}$$

4. Tool – workpiece engagement model and Cutter Engagement Boundary (CEB) identification

CEB is defined as the tool-workpiece engagement region at each elevation in cylindrical coordinates. Three separate conditions must be evaluated at each level to determine the total engagement boundary. These conditions are uncut chip load condition, radial workpiece boundary and axial workpiece boundary. For each condition, the possible cutting points with respect to this specified limitation is kept as an array of Boolean input designating whether a point is in cut or not. Finally employing a union operation considering all of the generated Boolean arrays through separate cutting conditions, for each axial cross-section considering all three arrays the points in cut are found.

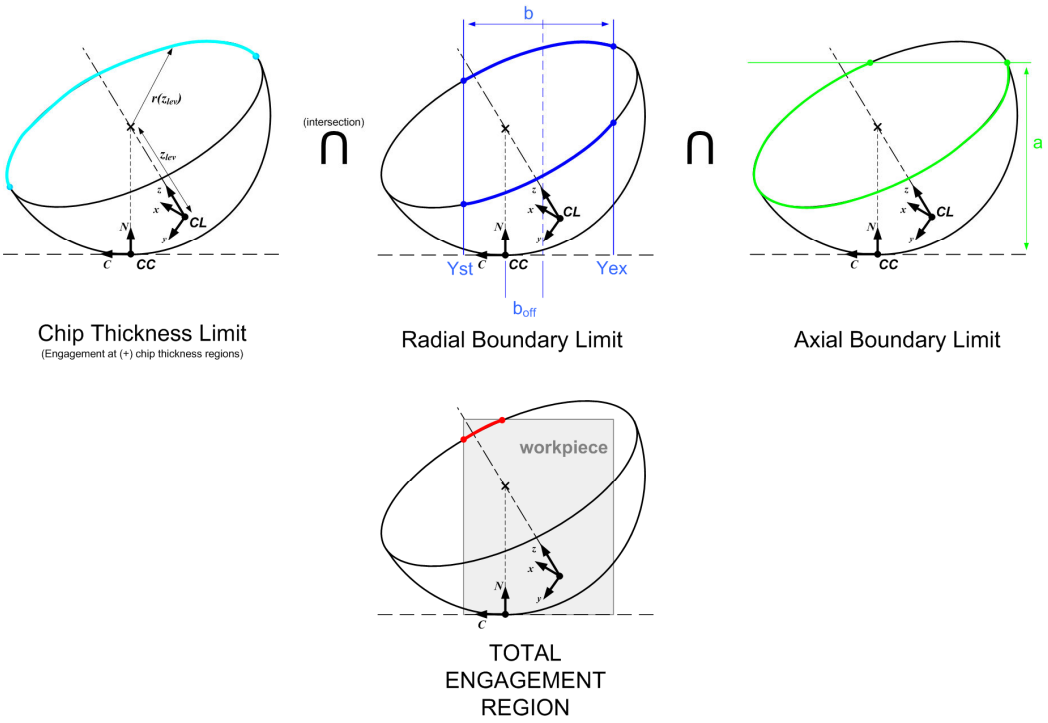

Fig. 9. Engagement boundary conditions and total engagement

A point on the tool periphery may only cut if there exists un-removed material in the feed direction, F . In Fig. 8, the gray shaded area in Section A-A designates the material to be cut at that axial level for a full revolution of the tool. For each axial level along the tool axis the portion of the tool cross-section in contact with the material can then be found by determining points which have positive-signed chip thickness, $h(\phi_j, z)$. Secondly, the radial workpiece boundaries are evaluated to find possible tool points in cut. Workpiece thickness is defined as b whereas the offset of the workpiece center line with respect to the normal direction N in the positive cross-feed direction is defined as b_{off} . Thus, start and finish boundaries of the workpiece in radial direction is expressed as:

$$Y_{ex} = b_{off} - b/2$$
$$Y_{st} = b_{off} + b/2 \qquad (24)$$

Possible points in cut are then identified whether they lie between these two limit lines ($Y_{st} \le P_C \le Yex$). The final condition for possible cutting points is to determine the ones below the axial depth of cut a ($P_N \le a$).

For a sample case, the engagement boundary simulation is demonstrated in Fig. 10. The chosen three-fluted taper ball end mill has 8 mm ball diameter, 10° single side taper angle and 30° constant helix angle. Radial depth of cut b and radial offset b_{off} is set to 10mm and 2mm respectively and axial depth of cut a is chosen as 10 mm. Tool is rotated and tilt and lead angles are set as 25° and 30° respectively.

5. Model Validation

Multi-axis cutting experiments were conducted to validate the proposed model with different tool types for varying cutting conditions. As a sample case, a 5-axis operation with a ball end cutter is examined. The process involves cutting of a Ti_6Al_4V workpiece with a two fluted, 6 mm diameter ball end tool. Orthogonal database provided by Budak et al. [1996] is utilized to predict milling force coefficients. The tool is positioned with +10^o lead and -15^o tilt angles. Feed rate and the spindle speed are 0.1 mm/tooth and 3000 rpm respectively. Axial depth is set as 1.5 mm and a slotting case is simulated. Simulation axial discretization step size is taken as 0.025 mm. Simulated and measured forces acting on the tool in process coordinates are compared in Fig. 11.

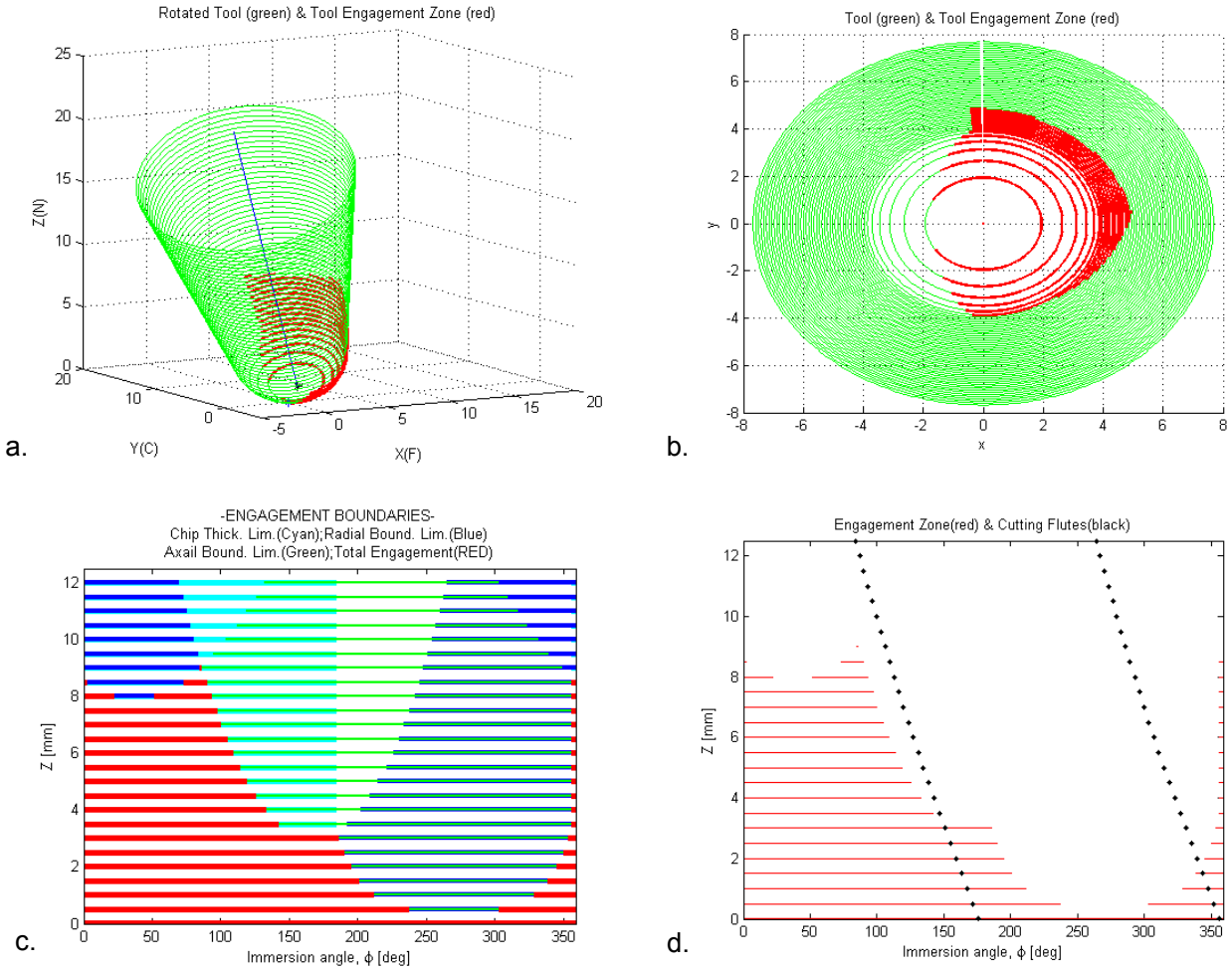

Fig. 10. CEB simulation for a sample case showing: (a-b) 3D rotated cutting tool with engaged region in red, (c) CEB union conditions together, and (d) total engagement boundary with axial cutting flute points on the unfolded cutter surface.

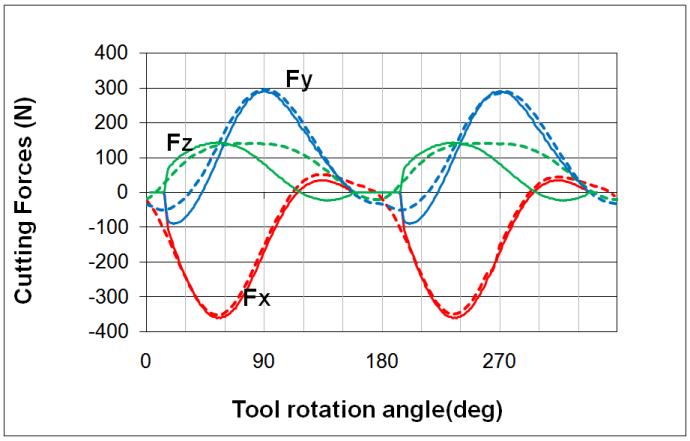

Fig. 11. Simulated versus measured forces (simulated in thin line, measured in dashed).

For this case the results showed that the proposed model predicts forces in feed and cross-feed directions accurately whereas the forces in the normal direction deviate from measured data, however maximum values are predicted reasonably closely.

6. Conclusion

In this paper, a numerical model to calculate forces in multi-axis machining using general tool geometries is proposed. In this method, the cutter-workpiece engagement regions are identified as discretized points on the tool periphery defined in cylindrical coordinates. The engagement boundary is determined with respect to three limitations; the sign of the calculated chip thickness, radial and axial boundary limits. . With this proposed methodology, cutting forces for generalized tool geometry in multi-axis milling can be identified accurately. As future work, the model is planned to be extended to analyze dynamics of cutting to obtain stability lobes. The model will also be used for virtual cutting process simulation of a complete machining cycle.

REFERENCES

1. **Budak, E. et al. (1996)**, “Prediction of Milling Force Coefficients From Orthogonal Cutting Data.”, Journal of Manufacturing Science and Engineering, Vol.118, pp 216-225.

2. **Choi, B.K. and Jerard, R.B. (1998),** Sculptured Surface Machining: Theory and Applications, Kluwer Academic Publishers, The Netherlands.

3. **Engin, S. and Altıntaş, Y. (2001),** “Mechanics and Dynamics of General Milling Cutters. Part I: Helical End Mills”, Int. Journal of Machine Tools & Manufacture. Vol.41, pp 2195-2212.

4. **Ferry, W. B.S. (2008),** “Virtual 5axis flank milling of jet engine impellers”, Ph.D. Thesis, University of British Columbia Mechanical Enginnering Program, Vancouver, Canada.

5. **Gradisek, J. et al. (2004),** “Mechanistic Identification of Specific Force Coefficients for a General End Mill”, Int. Journal of Machine Tools & Manufacture, Vol.44, pp 401-414.

6. **Kim, G.M. et al. (2000),** “Cutting Force Prediction of Sculptured Surface Ball-end Milling using Z-map”, Int. Journal of Machine Tools & Manufacture, Vol.40, pp 277-291.

7. **Lazoglu, I. and Liang, S.Y. (2000),** “Modeling of ball-end milling forces with cutter inclination”, Journal of Manufacturing Science and Enginnering, Vol.122, pp 3-11.

8. **Lee, P. and Altintas, Y. (1996)**, “A General Mechanics and Dynamics Model for Helical End Mills”, Annals of the CIRP, Vol.45, pp 59-64.

9. **Maeng, S.R. et al. (2003),** “A Z-map Update Method for Linearly Moving Tools”, Computer-Aided Design, Vol.35, pp 995-1009.

10. **Martelotti, M.E. (1941),** “An Analysis of Milling Process”, Transactions of ASME, Vol.63, pp 667-700.

11. **Merdol, S.D. and Altintas,Y. (2008),** “Virtual Simulation and Optimization of Milling Operations – Part I: Process Simulation”, Journal of Manufacturing Science and Engineering, Vol.130.

12. **Ozturk, E. and Budak, E. (2007),** “Modeling of 5-Axis Milling Processes”, Machining Science and Technology, Vol.11, pp 287-311.

13. **Zhu, R. et al. (2001),** “Mechanistic Modeling of the Ball End Milling Process for Multi-Axis Machining of Free-Form Surfaces”, Journal of Manufacturing Science and Engineering, Vol.123, pp 369-379.

14. **Kim, Y.H. and Ko, S.L (2006)**, “Improvement of Cutting Simulation Using the Octree Method”, Int. Journal of Advance Manufacturing Technology, Vol.28, pp 1152-1160.

15. **Kline, W.A. et al. (1982), “**The prediction of cutting forces in end milling with application to cornering cuts”, Int. Journal of Machine Tool Design and Research, Vol.22, pp 7-22

16. **National Bureau of Standarts,** “Digital Representation for Communication of Product Definition Data”, NBSIR 80-1978, 1980

17. **Altintas, Y. and Spence, A. (1991), “**End milling force algorithms for CAD systems”, CIRP Annals, Vol.40, pp 31-34